The Astrophysical Journal, 639:311–315, 2006 March 1

PROMPT OPTICAL OBSERVATIONS OF GRB 050319 WITH THE *SWIFT* UVOT

K. O. Mason,[1] A. J. Blustin,[1] P. Boyd,[2] S. T. Holland,[2] M. J. Page,[1] P. Roming,[3] M. Still,[2] B. Zhang,[4] A. Breeveld,[1] M. de Pasquale,[1] N. Gehrels,[2] C. Gronwall,[3] S. Hunsberger,[3] M. Ivanushkina,[3] W. Landsman,[2] K. McGowan,[1] J. Nousek,[3] T. Poole,[1] J. Rhoads,[5] S. Rosen,[1] and P. Schady[1]

Received 2005 June 16; accepted 2005 October 27

ABSTRACT

The UVOT telescope on the *Swift* observatory has detected optical afterglow emission from GRB 050319. The flux declined with a power-law slope of $\alpha = -0.57$ between the start of observations some 230 s after the burst onset (90 s after the burst trigger) until it faded below the sensitivity threshold of the instrument after $\sim 5 \times 10^4$ s. There is no evidence for the rapidly declining component in the early light curve that is seen at the same time in the X-ray band. The afterglow is not detected in UVOT shortward of the *B* band, suggesting a redshift of about 3.5. The optical *V*-band emission lies on the extension of the X-ray spectrum, with an optical-to-X-ray slope of $\beta = -0.8$. The relatively flat decay rate of the burst suggests that the central engine continues to inject energy into the fireball for as long as a few $\times$ 10^4 s after the burst.

Subject headings: astrometry — galaxies: distances and redshifts — gamma rays: bursts — shock waves — X-rays: individual (GRB 050319)

Online material: color figures

1. INTRODUCTION

The *Swift* observatory (Gehrels et al. 2004) is designed to localize gamma-ray bursts on the sky rapidly and then bring its X-ray and ultraviolet/optical telescopes to bear on that location within about 1 minute to provide panchromatic observations of the bursts and their afterglows. Initial information on the burst location and properties is transmitted to the ground in near-real time for distribution to follow-up observers. In this paper we describe *Swift* observations of the burst GRB 050319, concentrating on the data from the Ultraviolet/Optical Telescope (UVOT).

2. OBSERVATIONS AND ANALYSIS

The *Swift* Burst Alert Telescope (BAT; Barthelmy et al. 2005) triggered on the gamma-ray burst GRB 050319 at 09:31:18.44 UT (Krimm et al. 2005a). The burst light curve was initially reported as having a single peak with duration $T_{90} = 10 \pm 2$ s (Krimm et al. 2005b). However, subsequent analysis has shown that this was a multipeaked burst that actually began about 138 s before the *Swift* trigger (Fig. 1). The burst exhibits several peaks during an initial period of about 80 s, followed by a similar-length interval during which the BAT flux is indistinguishable from background, and then the final peak that generated the BAT trigger. The BAT did not trigger on the earlier activity because the spacecraft was slewing; triggers are disabled during slews. The slew ended about 50 s before the final peak. The energy index of the 1 s peak spectrum (starting at the trigger time, *T*, +0.36 s) is $\beta = -1.1 \pm 0.3$ (90% confidence; β defined such that $f_\nu \propto \nu^\beta$). The time-averaged spectrum of the final peak yields an energy index of -1.2 ± 0.2 (Krimm et al. 2005b).

The *Swift* spacecraft executed a slew immediately to bring the narrow-field X-Ray Telescope (XRT; Burrows et al. 2005) and UVOT (Roming et al. 2005) to bear on GRB 050319, and observations with these started about 90 s after the burst trigger (230 s after the burst onset). In this paper we concentrate on the analysis of the UVOT data and compare with the results from the XRT observations reported by Cusumano et al. (2006). We also consider data from a number of ground-based observatories that responded to the *Swift* trigger (Yoshioka et al. 2005; Quimby et al. 2005; Kiziloglu et al. 2005; Misra et al. 2005; Sharapov et al. 2005a, 2005b; Greco et al. 2005; Woźniak et al. 2005). The earliest observations were made 27 s after the *Swift* trigger (Quimby et al. 2005).

2.1. *Optical Decay*

The *Swift* UVOT executed a standard series of exposures, the first of which was a "finding chart" exposure of duration 100 s in the *V* filter that began 90 s after the BAT trigger. Thereafter, the instrument cycled through each of six color filters, *V*, *B*, and *U*, together with filters defining three ultraviolet passbands, UVW1, UVM2, and UVW2 (see Table 2 for central wavelengths). The exposure duration per filter was initially 10 s, subsequently increasing to 100 s and then 900 s at predetermined times after the trigger. The initial data (up to 1700 s after the trigger) were taken in "event mode," in which the time and detector position of each individual photon is recorded. For the later exposures, the instrument was switched to "image mode," in which the image is accumulated on board to conserve telemetry volume, discarding the photon-timing information within an exposure. The intrinsic spatial pixel size of the detector is approximately 0.″5 on the sky, but the image mode data were taken with the data binned 2×2 to give 1″ pixels.

Examination of the UVOT finding chart exposure reveals a new source within the XRT positional error circle of the burst (Krimm et al. 2005a) at R.A. = $10^{\rm h}16^{\rm m}47^{\rm s}.76(3)$, decl. = $+43^\circ 32' 54''.9(5)$ (J2000.0). The source fades with time, demonstrating that it is the afterglow of the burst. It has a mean *V* magnitude of 17.5 during the exposure, which is centered 140 s after the burst trigger (278 s after burst onset). The position of the

[1] Mullard Space Science Laboratory, Department of Space and Climate Physics, University College London, Holmbury St. Mary, Dorking, Surrey, RH5 6NT, UK; kom@mssl.ucl.ac.uk.
[2] NASA Goddard Space Flight Center, Greenbelt, MD 20771.
[3] Department of Astronomy and Astrophysics, Pennsylvania State University, 525 Davey Laboratory, University Park, PA 16802.
[4] Department of Physics, University of Nevada, Las Vegas, NV 89154.
[5] Space Telescope Science Institute, 3700 San Martin Drive, Baltimore, MD 21218.

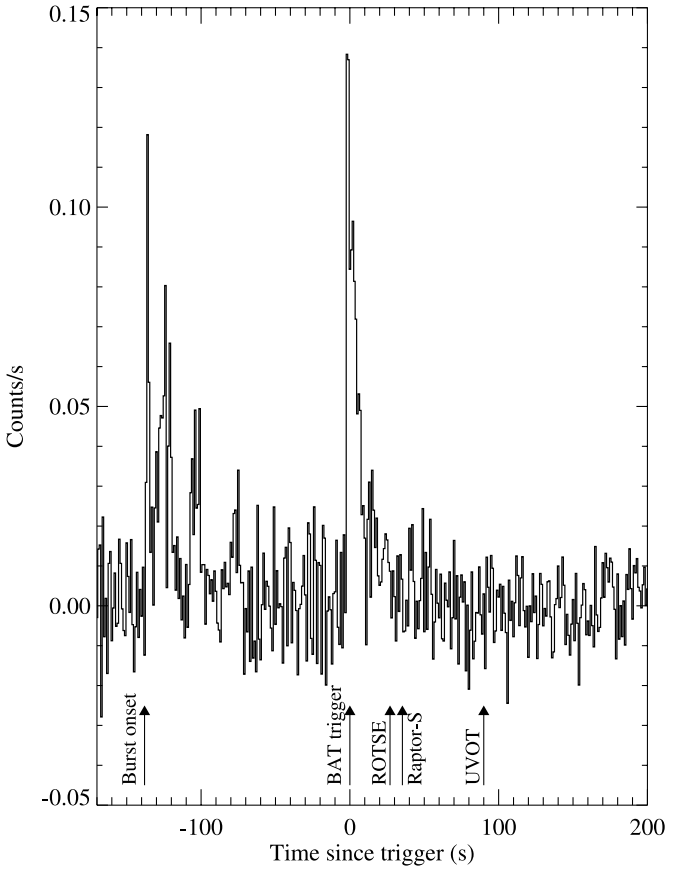

FIG. 1.—BAT mask-weighted light curve of GRB 050319 in the 15–350 keV band at 1 s time resolution. The burst began 138 s before the BAT trigger, which occurred on the final peak of the burst. The spacecraft was slewing at the time of the previous peaks, and BAT triggers are disabled during slews. The slew ended about 50 s before the trigger. The start of coverage from the ROTSE (Quimby et al. 2005) and RAPTOR-S (Woźniak et al. 2005) ground-based robotic telescopes and the *Swift* UVOT are marked.

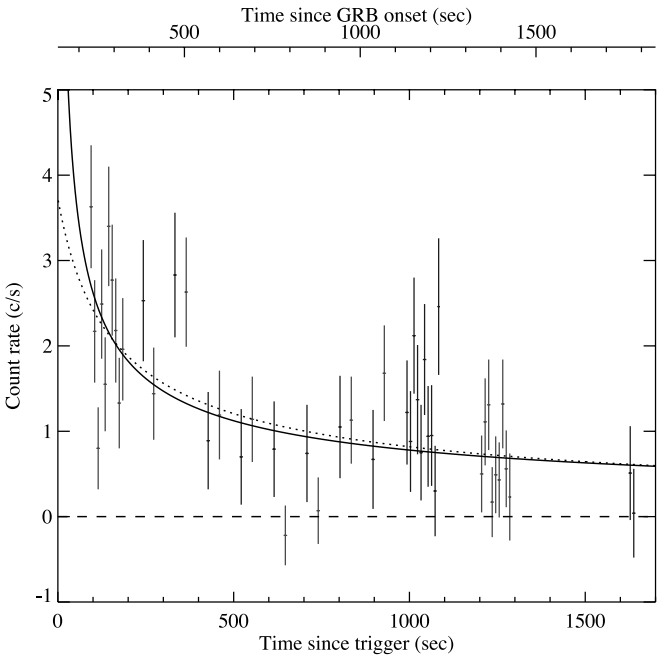

FIG. 2.—UVOT *V*-band and *B*-band count rate data in the interval up to 1700 s after the burst trigger. Since, as explained in the text, the burst began about 138 s before the trigger, we indicate time since burst onset on the upper axis. The *B*-band data have been multiplied by a factor of 0.8 to normalize them to the *V*-band (see text). The solid curve is the best-fit power-law decay curve, which has $\alpha = -0.57$. The dashed curve is a fit in which the time of origin of the power law, T_0, is allowed to be a free parameter (see text). [*See the electronic edition of the Journal for a color version of this figure*.]

afterglow is consistent with that reported by Rykoff et al. (2005). The afterglow is also seen in the UVOT *B* filter, in which the first observation is a 10 s exposure centered 243 s after the trigger. It is not present in observations made with any of the shorter wavelength UVOT filters taken around the same time.

The brightness of the afterglow was measured by extracting the counts from a circular aperture of 6″ radius centered on the source position. The background was measured from an annular region surrounding the source that had an inner radius of 6″ and an outer radius of 30″. Pixels in the background region that were significantly above the mean (due, for example, to the presence of another star) were rejected. The background count rate varies with Earth aspect angle, but is typically 0.01 counts s^{-1} $arcsec^{-2}$ in *V* and 0.02 counts s^{-1} $arcsec^{-2}$ in *B*. In Figure 2 we show the earliest UVOT data, plotted as a detector count rate on a linear scale in 10 s bins. These data, taken in event mode, extend to 1700 s after the trigger. We include both the *V*- and *B*-band data. By coincidence the count rate in the two filters is very similar, the greater transmission of the instrument in the *B* band being compensated for by the fact that the source is brighter in *V*. If we compare the count rate in the interval 250–950 s after the trigger, when the instrument was cycling often through the two filters, we get a mean count rate of 1.05 ± 0.18 counts s^{-1} in *V* and 1.31 ± 0.22 counts s^{-1} in *B*. These are consistent within the 1 σ error bounds, but we have multiplied the *B*-band data in Figure 2 by the mean factor of 0.8 for consistency. A power-law fit to the

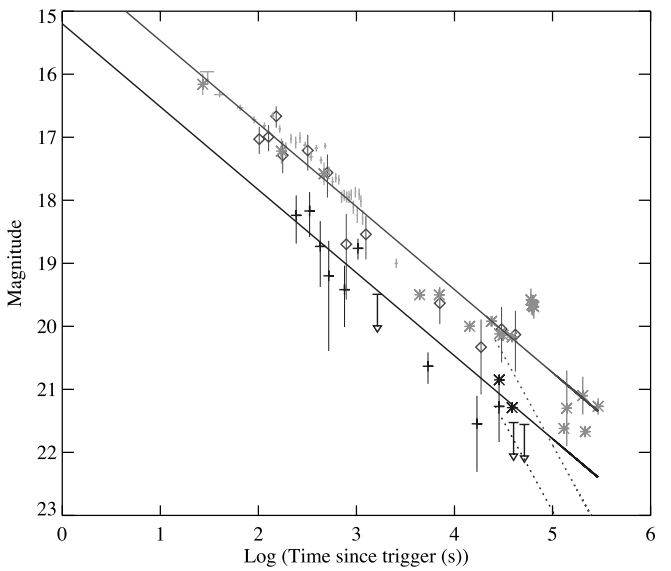

FIG. 3.—Measurements of the GRB 050319 afterglow decay plotted as magnitudes vs. the log of the time interval since the burst trigger. UVOT *V*-band (*diamonds*) and *B*-band (*big crosses*) magnitudes are compared against ground-based data reported in the literature (see text). The ground-based data are predominantly *R*-band, or equivalent *R*-band, measurements (*light gray asterisks*), but two ground-based *B*-band measurements (*dark gray asterisks*) are also shown. We also show the equivalent *R*-band measurements of the early afterglow reported by Woźniak et al. (2005; *small crosses*). A power-law decay curve with a slope $\alpha = -0.57$ is compared to the *V* and *B* data. The dashed lines show a break to an $\alpha = -1.14$ slope, as suggested by analysis of the X-ray data on this burst (Cusumano et al. 2006). [*See the electronic edition of the Journal for a color version of this figure*.]

TABLE 1
UVOT Time-Resolved Photometry

Mid Time[a] (s)	Exposure Time (s)	Magnitude	Error (mag)
	V Band		
102	25	17.03	0.22
127	25	16.99	0.21
152	25	16.67	0.17
177	25	17.28	0.26
319	20	17.21	0.28
506	20	17.56	0.34
788	40	18.70	0.69
1249	100	18.54	0.35
7088	700	19.65	0.29
18,664	689	20.35	0.57
30,217	726	20.07	0.42
41,791	718	20.09	0.43
	B Band		
243	10	18.24	0.38
333	10	18.17	0.36
428	10	18.73	0.52
522	10	19.19	0.86
756	40	19.42	0.48
1036	100	18.76	0.17
1637	26	>19.5	
5370	900	20.63	0.25
16,951	900	21.54	0.60
28,491	897	21.27	0.47
40,064	900	>21.5	
51,638	900	>21.5	

[a] Time since 2005 March 19, 9:31:18.44.

combined *V*- and *B*-band data, shown as a solid line in the figure, has a slope of $\alpha = -0.57 \pm 0.07$. We have included the UVOT data points beyond 1700 s in this fit. The origin of the power law in this treatment, T_0, is taken to be the time of the BAT trigger. However, as noted above, the burst actually began about 138 s before the trigger, so the appropriate value of T_0 is debatable. We have fit the data, allowing T_0 to be a free parameter, which yields $T_0 = -54 \pm 73$ s, and a slightly steeper slope of $\alpha = -0.63 \pm 0.08$. This fit is shown as a dashed line in Figure 2, but is statistically indistinguishable from the $T_0 = 0$ case. The reduced χ^2 value for the power-law fit to the time evolution data in 10 s bins is 0.75 per dof, which is statistically acceptable.

Figure 3 shows the *B* and *V* magnitude of the afterglow as a function of time since the trigger. The data, listed in Table 1, have been binned in time with respect to Figure 2 to increase the signal-to-noise ratio. The instrumental count rates are converted to magnitudes and fluxes using preliminary on-orbit calibration data, which might be subject to slight revision as calibration knowledge improves. The zero points used are listed in Figure 2. The magnitudes quoted here differ significantly, particularly in the *V* band, from those reported by Boyd et al. (2005), which were derived before on-orbit calibration data were available and were therefore based only on ground calibration estimates of the zero points. The UVOT magnitude system is defined such that the magnitude of Vega would be zero in each filter.

The $\alpha = -0.57$ power law derived above is compared to both the *V*- and *B*-band data in Figure 3. Both wavebands are consistent with the same overall slope. Specifically, the UVOT data indicate a $B - V$ color of $\sim$1, with no evidence of systematic evolution with time. We also show ground-based telescope data reported by Yoshioka et al. (2005), Quimby et al. (2005), Kiziloglu et al. (2005), Misra et al. (2005), Sharapov et al. (2005a, 2005b), Greco et al. (2005), and Woźniak et al. (2005), most of which report *R*-band or broadband measurements referenced to the *R*-band magnitudes of field stars. Comparison of these data with those from UVOT suggest that $V - R \sim 0$. However, we caution that the transformation of broadband measurements into standard color systems by reference to field stars is subject to systematic uncertainty, particularly when, as in this case, the intrinsic spectrum of the object of interest is likely to be different from that of the average field star.

It is interesting that the decay slope derived from the UVOT data extrapolates well to the early measurements of Quimby et al. (2005) and Woźniak et al. (2005); the former authors find that $R = 16.16 \pm 0.17$ 27 s after the *Swift* trigger, while the latter quote $R = 16.323 \pm 0.046$ 40 s after the trigger. Woźniak et al. (2005) find that there are systematic deviations from a simple power law during the early decline phase. Although they are of lower statistical quality, the UVOT data are very consistent with these data in suggesting an excess above the power law in the interval 200–800 s after the trigger. Woźniak et al. fit a broken power-law decay to their data (with $T_{\rm brk} \sim 400-500$ s). However, the later UVOT and ground-based measurements suggest that these deviations can be characterized as fluctuations about a mean $\alpha \sim -0.5$ slope.

At late times, analysis of the *Swift* XRT data by Cusumano et al. (2006) indicate that there is a break in the X-ray light curve of GRB 050319 at about 2.6×10^4 s from a slope consistent with that of the optical data to one with $\alpha = -1.14$. Such a break is indicated in Figure 3 for illustration. While the UVOT data do not constrain the presence of such a break, the late ground-based optical data seem to favor an extension of the $\alpha = -0.5$ slope.

2.2. *Spectrum*

To examine the spectrum of GRB 050319, we use data from the interval between 240 and 930 s after the trigger, when the

TABLE 2
UVOT Spectral Photometry: T + (240–930 s)

Filter	Effective Wavelength (Å)	Integrated Exposure (s)	Counts s^{-1}	Zero Point (10^{-16} ergs cm^{-2} s^{-1} Å^{-1})	Flux (10^{-16} ergs cm^{-2} s^{-1} Å^{-1})
V	5430	80	1.05 ± 0.18	2.64	2.76 ± 0.48
B	4340	80	1.31 ± 0.22	1.33	1.75 ± 0.29
U	3440	90	<0.36	1.54	<0.54
UVW1	2600	90	<0.15	3.37	<0.46
UVM2	2200	90	<0.09	7.60	<0.72
UVW2	1930	80	<0.09	4.94	<0.50

Notes.—Upper limits are quoted at 3 σ. The zero point is the flux corresponding to 1 count s^{-1}.

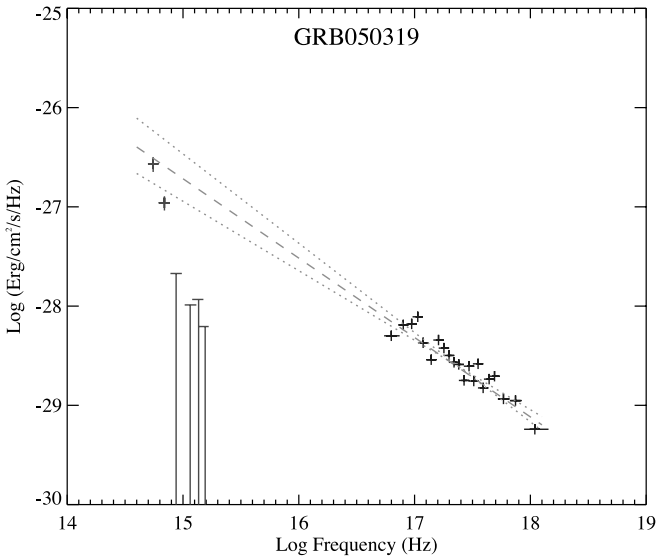

FIG. 4.—Multiwavelength spectrum of GRB 050319 plotted as $F\nu$ vs. log frequency in the observer frame, and averaged over the interval between 240 and 930 s after the burst trigger. UVOT data points are shown in light gray, XRT data in dark gray. The best power-law fit to the XRT data is illustrated as the dashed line. The 1 σ bounds on the slope are indicated by the dotted lines. The XRT flux points have been corrected for Galactic absorption equivalent to $N_{\rm H} = 1.17 \times 10^{20}$ cm^{-2}. [*See the electronic edition of the Journal for a color version of this figure.*]

UVOT was cycling through each of its six color filters with exposure times of 10 s per filter, ensuring that the data from each filter sampled the same portion of the decay light curve. The filter wheel was rotated 8.5 times during this interval, yielding eight observations in the *V*, *B*, and UVW2 filters, and nine each in *U*, UVW1, and UVM2. The mean count rate and flux, or 3 σ limit on these quantities, is listed in Table 2. The spectral flux distribution is shown in Figure 4. Reddening due to the Galaxy in the direction of the burst is very low. At $A_V = 0.034$ (Schlegel et al. 1998), no correction is applied in the plot.

We also show X-ray data from the *Swift* XRT averaged over exactly the same time interval as the UVOT data. The count data derived from the XRT during this time period are fitted to a power-law spectrum absorbed by a fixed Galactic absorbing column of $N_{\rm H} = 1.17 \times 10^{20}$ cm^{-2}. The best-fit spectrum has a slope (β) of -0.8 ± 0.1. This fit is used to convert the count rate data to incident flux, and these data are then plotted in Figure 4, corrected for the Galactic absorption, to compare with the UVOT measurements.

A simple power-law extrapolation of the XRT X-ray spectrum predicts the *V*-band flux well. However, the UVOT *B*-band measurement at 435 nm and the upper limits to the flux in the *U*, UVW1, UVM2, and UVW2 filters, which cover the wavelength range 180–390 nm, lie significantly below any reasonable distribution joining the *V*-band and X-ray data. The *B*-band flux falls below the power law joining the X-ray to the *V* band by a factor of $\sim$2. This suggests that the optical spectrum is cut off in the *B* band. If this is solely due to the Lyman edge at 91.2 nm in the rest frame, the implied redshift of the burst is $\sim$3.8. This is effectively an upper limit to the burst redshift, since there may be additional sources of opacity in the spectrum longward of the Lyman edge. For example, Lyα absorption in the host galaxy or the Lyman forest could contribute to the flux deficit. Fynbo et al. (2005) report an absorption-line system at a redshift of 3.24 in the spectrum of the afterglow. This would imply a Lyman edge at 387 nm, shortward of 97% of the response of the UVOT *B*-band filter. The absorption-line system is not necessarily due to the host galaxy of the burst, so conservatively we could bracket the burst redshift between 3.24 and $\sim$3.8. However, the UVOT data would be consistent with a host galaxy redshift of 3.24, provided that there is indeed significant additional absorption, due to Lyα for example, in the *B* band. Based on the intergalactic medium (IGM) transmission model of Madau (1995), the transmission through the *B* filter is consistent with $z = 3.24-3.5$ at the ± 1 σ level, and with $z < 3.8$ at the 3 σ level.

3. DISCUSSION

The UVOT instrument detected and followed the optical afterglow of GRB 050319 from when it was acquired by the *Swift* narrow-field instruments, about 90 s after the burst trigger, until it faded below the UVOT sensitivity threshold, about 50,000 s later. The afterglow was detected in the *V* and *B* bands, but not at shorter wavelengths. Interpreting this spectral cutoff as being due to the Lyman edge of hydrogen suggests an upper limit to the burst redshift of $\sim$3.8. This is consistent with the reported absorption line system at $z = 3.24$ (Fynbo et al. 2005), which is likely to be the host galaxy of the burst. There is no evidence for significant evolution of the $B - V$ color as a function of the burst decay (Fig. 3).

The multiwavelength spectrum of the afterglow, derived from the interval between 240 and 940 s after the trigger, suggests that the observed *V*-band flux (which is at a wavelength of $\sim$1300 Å in the rest frame of the burst) is an extension of the $\beta = -0.8 \pm 0.1$ X-ray spectral distribution. Indeed, the combined X-ray and *V*-band data are perfectly consistent with this slope. The interval used to compile this spectrum begins just after the first break in the X-ray time evolution curve (see below) as reported by Cusumano et al. (2006). The X-ray spectrum before this break is significantly softer ($\beta = -1.6$) than after ($\beta = -0.7$), and the interval used for the X-ray spectrum in Figure 4 may be slightly contaminated by the remnants of the soft component. However, Cusumano et al. derive a weighted average spectral slope for all the X-ray data after this break of $\beta = -0.73 \pm 0.05$, which is consistent with our X-ray to *V*-band slope within errors, suggesting that any such contamination is minor. The multiwavelength spectrum of GRB 050319 is in accord with expectations from the relativistic fireball model (e.g., Granot & Sari 2002) and suggests that a single optically thin synchrotron afterglow spectrum extends from the X-ray to the (rest-frame) UV band. This idea is supported by the fact that the mean optical decay slope is indistinguishable from the decay slope of the X-ray flux in the interval between about 230 s and 2.7×10^4 s after the trigger, which is $\alpha = -0.51 \pm 0.03$ (Cusumano et al. 2006).

The optical flux decays with a mean power law slope of $\alpha = -0.57 \pm 0.07$, but there is good evidence for fluctuations from this steady decline, from the UVOT and particularly from the well-sampled early phase coverage of Woźniak et al. (2005). Such variability might be due to fluctuations in the density of the circumburst medium, or to continued injection of relativistic material into the fireball (refreshed shock). The shallow overall decay slope combined with the observed spectral slope would require an unusually flat electron energy spectral index in the context of the simple fireball model (e.g., Granot & Sari 2002). However, the idea that the central engine is continuously injecting energy into the fireball may be a more natural explanation of the shallow decay. If we parameterize the injection as producing a luminosity $L \propto t^{-q}$, this continuous injection would influence the dynamics of the fireball, and hence the light curves, as long as $q < 1$ (Zhang & Mészáros 2001). Assuming that the central engine stops injecting energy after 2.7×10^4 s, we get a consistent solution for the UVOT and XRT light curve with q in the range 0.5–0.6 and $p \sim 2.8$. Both the optical and X-ray bands are

between the injection frequency ν_m and the cooling frequency ν_c throughout. This is satisfied within a wide parameter regime.

Interestingly, prior to $T+230$ s the X-ray flux decays much more steeply, with a power-law slope of $\alpha = -2.9 \pm 0.3$ (Cusumano et al. 2006). Thus, at $T+90$ s, when the burst was first acquired by the *Swift* narrow-field instruments, the X-ray flux was more than 20 times brighter than it was at $T+230$ s. There is no evidence for a similar rapidly decaying component in the flux measured with the UVOT, which would have needed to be at about 14 mag rather than the observed 17 mag at $T+100$ s to match the XRT data. Furthermore, the Robotic Optical Transient Search Experiment (ROTSE) and Rapid Telescopes for Optical Response (RAPTOR) data taken as early as 27 s after the BAT trigger (Quimby et al. 2005; Woźniak et al. 2005) are also consistent with an extrapolation of the $\alpha = -0.57$ UVOT decay profile to earlier times with no rapidly decaying component. This is firm evidence that the early X-ray afterglow light curve is composed of two distinct components. The steep decay is likely to be the tail emission from the internal shocks (mainly due to the so-called curvature effect; Kumar & Panaitescu 2000), while the shallow broadband decay component comes from the external shock afterglow.

Early rapid decay phases have now been seen in a number of bursts with the XRT (cf. Cusumano et al. 2006). Optical observations have been made while the gamma-ray burst is ongoing in two bursts thus far, GRB 990123 (Akerlof et al. 1999) and GRB 041219 (Vestrand et al. 2005). In the case of GRB 990123 the optical emission was not correlated in time with the gamma rays, peaking instead approximately 20 s after the gamma-ray emission. A possible explanation for the optical light in this case is that it arose in the reverse shock driven into the ejecta by interaction with the surrounding medium (Mészáros & Rees 1997; Sari & Piran 1999; Zhang et al. 2003). However, in the case of GRB 041219, the optical emission was well correlated with the gamma rays, suggesting that it arose due to internal shocks in the ultrarelativistic ejecta itself (Vestrand et al. 2005). If the rapidly decaying XRT flux in GRB 050319 is related to the prompt emission, then neither mechanism resulted in a detectable optical flash in GRB 050319. This might be due to various mechanisms that suppress the reverse-shock optical flash (e.g., Kobayashi 2000; Zhang & Kobayashi 2005), and to the strong synchrotron self-absorption effect during the prompt emission phase, which suppresses the internal-shock optical flash (Fan et al. 2005).

We thank John Cannizzo for supplying the BAT data that are used in Figure 1. The *Swift* program is supported by NASA, PPARC, and ASI.

REFERENCES

Akerlof, C., et al. 1999, Nature, 398, 400
Barthelmy, S. D., et al. 2005, Space Sci. Rev., 120, 143
Boyd, P., et al. 2005, GCN Circ. 3129, http://gcn.gsfc.nasa.gov/gcn/gcn3/3129.gcn3
Burrows, D. N., et al. 2005, Space Sci. Rev., 120, 165
Cusumano, G., et al. 2006, ApJ, 639, 316
Fan, Y. Z., Zhang, B., & Wei, D. M. 2005, ApJ, 628, L25
Fynbo, J. P. U., et al. 2005, GCN Circ. 3136, http://gcn.gsfc.nasa.gov/gcn/gcn3/3136.gcn3
Gehrels, N., et al. 2004, ApJ, 611, 1005
Granot, J., & Sari, R. 2002, ApJ, 568, 820
Greco, G., et al. 2005, GCN Circ. 3142, http://gcn.gsfc.nasa.gov/gcn/gcn3/3142.gcn3
Kiziloglu, U., et al. 2005, GCN Circ. 3139, http://gcn.gsfc.nasa.gov/gcn/gcn3/3139.gcn3
Kobayashi, S. 2000, ApJ, 545, 807
Krimm, H., et al. 2005a, GCN Circ. 3117, http://gcn.gsfc.nasa.gov/gcn/gcn3/3117.gcn3
———. 2005b, GCN Circ. 3119, http://gcn.gsfc.nasa.gov/gcn/gcn3/3119.gcn3
Kumar, P., & Panaitescu, A. 2000, ApJ, 541, L51
Madau, P. 1995, ApJ, 441, 18
Mészáros, P., & Rees, M. J. 1997, ApJ, 476, 232
Misra, K., et al. 2005, GCN Circ. 3130, http://gcn.gsfc.nasa.gov/gcn/gcn3/3130.gcn3
Quimby, R. M., et al. 2005, GCN Circ. 3135, http://gcn.gsfc.nasa.gov/gcn/gcn3/3135.gcn3
Roming, P. W. A., et al. 2005, Space Sci. Rev., 120, 95
Rykoff, E., Schaefer, B., & Quimby, R. 2005, GCN Circ. 3116, http://gcn.gsfc.nasa.gov/gcn/gcn3/3116.gcn3
Sari, R., & Piran, T. 1999, ApJ, 517, L109
Schlegel, D. J., Finkbeiner, D. P., & Davis, M. 1998, ApJ, 500, 525
Sharapov, D., et al. 2005a, GCN Circ. 3124, http://gcn.gsfc.nasa.gov/gcn/gcn3/3124.gcn3
———. 2005b, GCN Circ. 3140, http://gcn.gsfc.nasa.gov/gcn/gcn3/3140.gcn3
Vestrand, W. T., et al. 2005, Nature, 435, 178
Woźniak, P. R., et al. 2005, ApJ, 627, L13
Yoshioka, T., Chen, C. W., & Nishiura, S. 2005, GCN Circ. 3120, http://gcn.gsfc.nasa.gov/gcn/gcn3/3120.gcn3
Zhang, B., & Kobayashi, S. 2005, ApJ, 628, 315
Zhang, B., Kobayashi, S., & Mészáros, P. 2003, ApJ, 595, 950
Zhang, B., & Mészáros, P. 2001, ApJ, 552, L35